High Power Optical Pulses through Linear, Nonlinear, and Time-Varying Media and their Applications

A Thesis submitted by

Piyali Biswas

in partial fulfillment of the requirements for the award of the degree of

Doctor of Philosophy



Indian Institute of Technology Jodhpur
Department of Physics

April, 2023

Certificate

This is to certify that the thesis titled *High Power Optical Pulses through Linear, Nonlinear, and Time-Varying Media and their Applications*, submitted by *Piyali Biswas (P17PH003)* to the Indian Institute of Technology Jodhpur for the award of the degree of *Doctor of Philosophy*, is a bonafide record of the research work done by her under my supervision. To the best of my knowledge, the contents of this report, in full or in parts, have not been submitted to any other Institute or University for the award of any degree or diploma.



Somnath Ghosh
Ph. D. Thesis Supervisor

Declaration

I hereby declare that the work presented in this thesis entitled *High Power Optical Pulses through Linear, Nonlinear, and Time-Varying Media and their Applications* submitted to the Indian Institute of Technology Jodhpur in partial fulfillment of the requirements for the award of the degree of Doctor of Philosophy, is a bonafide record of the research work carried out under the supervision of Dr. Somnath Ghosh. The contents of this thesis in full or in parts, have not been submitted to, and will not be submitted by me to, any other Institute or University in India or abroad for the award of any degree or diploma.

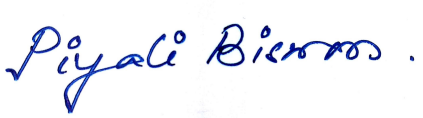

Piyali Biswas
P17PH003

Acknowledgment

First and foremost, I would like to express my utmost gratitude towards my research advisor Prof. Somnath Ghosh. The successful completion of this thesis has been made possible only with the continual guidance and encouragement I have received from him over the past five years. His relentless enthusiasm towards research has kept me motivated, while his outstanding technical knowledge and understanding of the subject have always helped me to acquire more out of the research work through our discussions. Moreover, he has shown me the path of professionalism and consciousness through his own actions by efficiently managing his time between research and his numerous administrative responsibilities, which would surely guide me in my future endeavors. I have been thankful to him for always providing me the time-to-time support, both intellectually and emotionally. I could not have imagined having a better advisor and mentor for my Ph.D study.

Besides, I would like to thank the rest of my thesis committee: Prof. Satyajit Sahu, Prof. Kirankumar R. Hiremath, and Prof. Soumava Mukherjee, for their insightful comments and encouragement, but also for the hard questions which certainly helped me to widen my research from various perspectives.

I am also grateful to meet and work with Prof. Bishnu P. Pal. His excellence in the domain of fiber optics and photonics has helped my thesis work to grow further. Every technical discussion with him has been the most delightful experience. Further, I would like to convey my gratitude towards Prof. Hai-Xiao Wang for sharing his knowledge and experience of working on topological devices which has been an important part of my thesis. The discussions we had, have certainly provided me the insight of the topic.

Next, I can only be thankful to my fellow laboratory mates and colleagues, Arnab Laha, Sayan Bhattacherjee, Suman Dey, Sibnath Dey, Snehashis Sadhukhan, Harsh K. Gandhi, and Arpan Roy with whom I have spent the maximum amount of time in this five years. The numerous discussions and debates on various technical aspects, as well as on basic subject matters has been undoubtedly the most enriching experience. I thank them for their generous help to overcome technical challenges related to my thesis work, for working hard together to meet the deadlines, and for all the fun we have had in the last five years.

My sincere thanks also goes to IIT Jodhpur fraternity who have provided me the space and resources to continue my research work throughout the five years. I am also thankful to I-STEM for providing me the technical support, and Ministry of Education (MoE), India to provide me the financial support over these five years.

Last but not the least, I would like to thank my parents and my sister for being my strength throughout the five years. And this list would not be complete without mentioning my companions, Jaspreet and Akhil, for being my support system at the home away from home.

Piyali Biswas.

Dedicated to Maa and Bapi.

Abbreviations

Abbreviation	Full Form
DDF	Dispersion Decresaing Fibers
DDBF	Dispersion Decresaing Bragg Fibers
DOBF	Dispersion Oscillating Bragg Fibers
EM	Electromagnetic
FDTD	Finite Difference Time Domain
GVD	Group Velocity Dispersion
IRS	Intrapulse Raman Scattering
MFD	Mode Field Diameter
NLS	Nonlinear Schrödinger
OWB	Optical Wave Breaking
PBG	Photonic Bandgap
PCF	Photonic Crystal Fibers
SBF	Specilaty Bandgap Fibers
SPM	Self-Phase Modulation
SSFM	Split-Step Fourier Method
SS	Self-Steepening
TIR	Total Internal Reflection
TMM	Transfer Matrix Method
TOD	Third Order Dispersion
TPA	Two-Photon Absorption
TTM	Time-Transformation Method
XPM	Cross-Phase Modulation

List of symbols

Symbol	Name
c	Speed of light in vacuum
n	Refractive index
ϵ_0	Free space permittivity
ϵ	Dielectric constant
μ_0	Free space permeability
μ	Permeability of medium
β	Propagation constant
α	Loss parameter
β_2	Group velocity dispersion parameter
D	Dispersion parameter
β_3	Third order dispersion coefficient
γ	Kerr nonlinear coefficient
$R(t)$	Raman response function
n_2	Nonlinear refractive index
α_2	Two-photon absorption coefficient
λ	Wavelength of light
ω	Angular frequency
ν	Frequency of light
k	Wave vector
K	Bloch wave vector

List of Figures

1.1 The schematic representation of dispersion-induced pulse broadening during propagation in a dielectric waveguide. 4

1.2 The schematic representation of nonlinearity-induced spectral broadening during propagation in a dielectric waveguide. 6

1.3 (a) Evolution of soliton from a sech input pulse form inside a 10 km long optical fiber, (b) Evolution of parabolic pulse from a Gaussian pulse as input through a 2 m long dispersion decreasing fiber, and (c) a dark similariton pulse with infinite background. 10

1.4 The schematic representation of (a) index guided PCF, (b) hollow-core bandgap guided PCF, and (c) all-solid Bragg fiber. 13

1.5 (a) The schematic representation of topological phase transition. The red arrows denote the sequential closing and re-opening of the operating bandgap under perturbation. The blue arrows denote the phase transition between the two bands adjacent to the operating bandgap. Also, the topological invariants of the bands are shown before and after the phase transition. (b) The schematic of the topological fiber cross-section based on 1D periodic lattice along with the interface state. 16

1.6 (a) The schematic representation of the linear time-varying medium in which at time t_b the refractive index of the medium n_1 is homogeneously changed to n_2. (b) The transmission and reflection of incident EM wave at the temporal boundary t_b along with the direction of respective wave-vectors. 20

1.7 The schematic representation of the thesis outline with the study-specific respective physical structures. 23

2.1 The schematic representation of the process of symmetrized-SSFM used for numerical simulations in optical fibers. The fiber length has been divided in segments of step-size h. Also, the nonlinearity is incorporated at the mid-planes of the segments only. The cyan colored arrow denotes the direction of pulse propagation. 36

2.2 The schematic illustration of an optical pulse propagating through a linear time-varying medium. The medium has been shown in a time scale where $n(t)$ represents an arbitrary refractive index change within the time span $T_i \rightarrow T_f$. The input pulse part shown by blue strip at time t' is delayed at the output of the linear time-varying medium by the time dependent delay $T_d(t')$. 39

3.1 The schematic illustration of a standard Bragg fiber cross-section along with the radial variation of the refractive index. 43

3.2 (a) The schematic of the designed Bragg fiber, (b) the variation of the confinement loss for the fundamental mode in the designed fiber 45

3.3 (a) the schematic representation of the longitudinally tapered fiber with input and output cross-sections, (b) the decreasing dispersion profile of the designed Bragg fiber. 46

3.4 (a) The evolution of a Gaussian pulse as input into an output parabolic one through 50 m long designed DDBF, (b) the developed linear frequency chirp (blue curve) across the entire width of the parabolic pulse (black curve) at the end of 50 m. . . . 47

3.5 (a) The input pulse profiles, (b) the output pulse profiles, (c) the logarithmic plots of the output pulses, and (d) the output chirp variations of the tanh-guided Gaussian pulse (blue curve) and the single Gaussian pulse (black curve) through the 4 km long designed DDBF. 48
3.6 (a) The input pulse profiles, (b) the output pulse profiles, (c) the logarithmic plots of the output pulses, and (d) the output chirp variations of the tanh-guided sech pulse (red curve) and the single sech pulse (grey curve) through the 4 km long designed DDBF. 49
3.7 The variation of misfit parameter M along the length of the DDBF for (a) tanh-guided Gaussian and a single Gaussian pulse, (b) tanh-guided sech and a single sech pulse. 51
3.8 The output spectra of (a) tanh-guided Gaussian and single Gaussian pulse, (b) tanh-guided sech and single sech pulse at the end of the 4 km long DDBF; (c) and (d) shows the closer look at the top of the respective spectral profiles. 52

4.1 (a) The schematic of the Bragg fiber cross-section designed at 2.8 μm, (b) the confinement loss spectrum of the fundamental mode in the designed Bragg cross-section as obtained from the modal analysis using TMM. 57
4.2 (a) The schematic of Fiber I which is a 2 m long down-tapered segment with input and output cross-sections. The corresponding longitudinal profiles of (b) GVD parameter β_2, and (c) nonlinear parameter γ. 58
4.3 (a) The schematic illustration of the Fiber II clubbing a 1 m long down-tapered section with a 1 m long up-tapered section to achieve oscillating dispersion profile. The corresponding longitudinal profiles of (b) GVD parameter β_2, and (c) nonlinear parameter γ over 6 m long Fiber II segment. 59
4.4 The longitudinal variations of (a) GVD parameter β_2, and (b) nonlinear parameter γ over 8 m long designed DOBF. 59
4.5 (a) The formation of parabolic pulse from an input Gaussian pulse, (b) the corresponding frequency chirp across the pulse width at various fiber lengths, and (c) the variation of misfit parameter M through the 8 m long chalcogenide glass based DOBF at 2.8 μm. 60
4.6 The evolution of (a) two consecutive input Gaussian pulses into output parabolic pulses, and (b) the corresponding frequency chirps across their pulse width through the DOBF; the evolution of (c) three consecutive input Gaussian pulses into output parabolic pulses, and (d) their corresponding frequency chirp through the DOBF; (e) the comb-like output spectrum at the end of the DOBF for three consecutive pulses. 62
4.7 (a) The spectral profiles at various lengths of the 8 m long DOBF in presence of higher order nonlinearity, and (b) the corresponding time-domain pulse profiles along with the frequency chirp developed across the pulse width as shown in the lower panel. . 64
4.8 (a) The longitudinal dispersion profile of the DDF, (b) the output spectral profiles at various lengths of the DOBF along with the output spectrum obtained at the end of the DDF (gray solid curve), and (c) the corresponding time-domain output pulse profiles. 65
4.9 (a) The profile of the TOD coefficient β_3 along the 8 m long DOBF, (b) the input and output pulse profiles up to 4 m of the DOBF in presence of TOD, and (c) the corresponding spectral evolution through the total fiber length. 66
4.10 (a) The schematic representation of the chirped-clad Bragg cross-section along with the aperiodic refractive index profile, (b) the input and output pulse profiles through the chirped-clad DOBF in presence of TOD, (c) the corresponding spectral evolution, and (d) the chirp profile at various length of the chirped-clad DOBF, (e) the misfit parameter evolution in presence of TOD for a standard DOBF and a chirped-clad DOBF. 67

4.11 (a) The input and output pulse profiles at various fiber lengths in presence of TOD, and (b) the corresponding chirp variation, (c) the spectral evolution through the chirped-clad DOBF at 1.06 μm. 69

5.1 (a) The schematic representation of the designed SBF-I showing three consecutive concentric cores namely **Core 1**, **Core 2**, and **Core 3**, where each core is guided by a set of specific combination of bilayer composed of a high index material followed by a low index material; (b) the cross-sectional refractive index profile is shown using two materials with refractive indices denoted by n_{high} and n_{low}. Λ_1, Λ_2, and Λ_3 are the chosen thicknesses of the bilayers which form the corresponding concentric cores having radii $\mathbf{R}_1$, $\mathbf{R}_2$, and $\mathbf{R}_3$, respectively. 75

5.2 The fundamental mode profiles from (a) TMM based numerical mode analysis, and (c) COMSOL simulation at the three operating wavelengths, 0.98 μm, 1.20 μm, and 2.10 μm, of the designed SBF-I. In (a), the solid black curve is the FM profile guided by the first bilayer Λ_1, dash-dotted curve for the Λ_2, and dotted curve for Λ_3; in (b) the overlapping of the bandgaps characterized by the three optimized bilayers are shown. 75

5.3 The confinement loss of the fundamental mode of the SBF-I geometry along with that of the counterpart standard Bragg fiber as a function of the wavelength. 77

5.4 The fundamental mode profiles denoted by blue solid, dashed and dash-dotted lines guided in the three consecutive concentric cores, respectively of the SBF-II geometry are shown in the upper panel along with the radial profile of the refractive index shown in the lower panel. 78

5.5 The confinement loss variation of the HE_{11} mode over the range of wavelength in SBF-II fiber. The inset shows the loss vs wavelength for the innermost core of the PBG fiber, with a kink corresponding to the overlapped region. Also, the two polarization of the HE_{11} mode has been shown. 79

5.6 The spectral variation of dispersion coefficient D and GVD parameter β_2 of the designed SBF-II. 80

5.7 The temporal and spectral evolution of the input Gaussian pulse through the SBF-II design in the normal dispersion regime are shown in figures (a) and (b), whereas their evolution through the same fiber in the anomalous dispersion regime are shown in figures (c) and (d), respectively. 81

5.8 (a) The lossless evolution of a 500 fs FWHM Gaussian pulse through the designed SBF-II in presence of anomalous dispersion and nonlinearity, (b) the time-domain output profiles of the pulse, and (c) the corresponding spectral profiles without loss and with loss at various fiber lengths. 82

5.9 (a) The lossless evolution of a 500 fs FWHM Gaussian pulse through the SBF-II in the presence of normal dispersion and nonlinearity, (b) the time-domain output pulse profiles and the chirp, and (c) the corresponding spectral profiles without loss (red curve) and with loss included (blue dotted curve) at the end of 2 km of the fiber length, (d) the evolution of the misfit parameter M over the fiber length along with the minimum misfit point shown by the red circle. 83

6.1 The schematic illustration of the topological specialty optical fiber based on 1D periodic lattices with inversion symmetry. The fiber comprises of two topologically distinct multi-layered cylinders owing to the thickness modulation of the periodic layers. Confinement of light will occur at the interface of the inner trivial and the outer nontrivial region as shown by the orange band. 88

6.2 (a) The 1D periodic lattice with the trivial topology. **A** and **B** are the low and high index materials, respectively and the blue dashed line denote the unit-cell of dimension a with inversion symmetry considered for the bandgap and Zak phase computation. (b) The variation of the operating bandgap with the change of the low-index layer thickness of the trivial lattice. The red dotted circle denotes the range of thickness of the low-index layer such that the chosen operating wavelength lies inside the trivial bandgap. 89
6.3 a) The photonic band structure of the 1D trivial lattice. The operating bandgap is shown by the cyan colored strip. Also, the Zak phases is inscribed for each energy band. (b) The corresponding reflection phase variation. The red dashed region corresponds to the operating bandgap of the trivial lattice. 90
6.4 (a) The 1D periodic lattice with the nontrivial topology. **A** and **B** are the low and high index materials, respectively and the blue dashed line denote the unit-cell of dimension a with inversion symmetry considered for the bandgap and Zak phase computation. (b) The variation of the operating bandgap with the change of the low-index layer thickness of the nontrivial lattice. The red dotted circle denotes the range of thickness of the low-index layer such that the chosen operating wavelength lies inside the nontrivial bandgap. 91
6.5 (a) The photonic band structure of the 1D nontrivial lattice. The operating bandgap is shown by the cyan colored strip. Also, the Zak phases is inscribed for each energy band. (b) The corresponding reflection phase variation. The red dashed region corresponds to the operating bandgap of the nontrivial lattice. 92
6.6 The reflectance plot of the composite lattice by clubbing 10 bilayers of trivial and 10 bilayers of nontrivial lattices alongside. The red arrow denotes the overlapped 1st higher order bandgap and the dip at the center of the bandgap indicates the existence of interface state at 1.56 μm. 93
6.7 The reflectance plot of the (10+10) lattice structure; (a) with an air defect in the trivial and nontrivial lattices separately, and (b) with the inclusion of 5% random correlated disorder in the lattice. 94
6.8 (a) The intensity plot of the transverse electric field localized at 1.56 μm in a (7+7) topological fiber; (b) the edge mode obtained from the mode analysis of the (7+7) geometry. 94
6.9 (a) The propagation of the interface state through the designed topological fiber. . . 95
6.10 The back-reflection free propagation of light in the topological fiber in presence of (a) a metal block, and (b) a dielectric block at the interface. 96
6.11 (a) The dispersion curves of the interface state including the waveguide and the material dispersion over the spectral range lying inside the topological bandgap. (b) The variation of GVD parameter β_2 over the spectral range of concern. 97
6.12 The temporal evolutions of a 500 fs Gaussian pulse with (a) 10 W, (c) 100 W, and (e) 1000 W peak power through the interface state inside the topological fiber; the corresponding spectral evolutions for (b) 10 W, (d) 100 W, and (f) 1000 W peak power in presence of Kerr nonlinearity only. 98
6.13 The output parabolic pulse in logarithmic scale along with the corresponding linear chirp at the end of 2.5 m of the topological fiber. 99

7.1 Schematic of the time-varying system with refractive index profile where t_b denotes the static temporal boundary coinciding with the vertical plane "B" of the bulk. Blue arrows denote the forward direction of pulse propagation while green arrows show backward propagation. 105
7.2 Time-domain input (dotted) and output pulse profile for forward (black) and backward (red) propagation in time-dynamic system. Inset shows the respective profiles for a time-static system. 106

7.3 Input (dotted) and output spectra for both forward (black) and backward (red) propagation in time-dynamic system. Similar profiles for time-static medium are shown as inset. . . . 107
7.4 Variation of instantaneous frequency with time for both forward (black) and backward (red) propagation. . . . 107
7.5 Logarithmic variation of forward transmission coefficient T_f and backward transmission coefficient T_b with related time-shift. . . . 108
7.6 Schematic of the time-dynamic system along with the time-varying refractive index profile. n_1 and n_2 are the complex refractive indices and the change of index occurs at time t_b corresponding to the plane B. Blue arrow refers to forward propagation whereas green arrow indicates backward propagation of pulse. . . . 109
7.7 Block diagram of the analytical model used to solve numerically the pulse propagation through the linear time-dynamic system using time-transformation approach. $E_{in}(t)$ is the input pulse which initially will undergo only time-transformation technique. The intermediate output $E'_{out}(t)$ will then be treated in frequency domain to include the effect of dispersion. $E_{out}(t)$ is the final output. . . . 110
7.8 Variation of input (dotted) and output pulse profiles with time for forward and backward propagation directions. . . . 111
7.9 Temporal output pulse profile with and without the inclusion of dispersion effect for (a) forward and (b) backward propagation directions. . . . 112
7.10 Variation of chirp with time during propagation in forward and backward direction. 112
7.11 Variation of input (dotted) and output spectral intensity with wavelength for both forward and backward propagation. . . . 113
7.12 Transmission profiles corresponding to forward and backward propagation directions, respectively depicting the asymmetric nature of light propagation. . . . 114
7.13 The time-varying refractive index profile for forward (blue) and backward (red) direction of propagation. The solid curves denote an abrupt change of index across the temporal boundary, whereas the dashed curves show their gradual change with time. 115
7.14 The variation of propagation constant β with frequency ν. The black and red solid curves show the variation of β in forward and backward propagation directions, respectively, before the time boundary. Similarly, the black and red dashed curves shows the same in forward and backward propagation directions, respectively, after the time boundary. The black and red arrows denote the change of β with time. . . . 117
7.15 Time-domain evolution of the 10 fs Gaussian pulse in (a) forward direction, and (b) backward direction of propagation for a relative index change of 0.2; the propagation distance is the length that can be traversed by the pulse within its time frame. . . . 117
7.16 (a) The spectra of the 10 fs input Gaussian pulse (gray dashed), the output pulse in the forward propagation direction (black solid), and the output pulse in the backward direction (red dash-dotted). (b) The variation of spectral nonreciprocity measured in dB with frequency. The black arrow shows the input pulse frequency. **F** and **B** denotes the position of shifted frequencies in the forward and backward direction of propagation, respectively. . . . 118